Security Classification

DOCUMENT CONTROL DATA - R & D

(Security classification of title, body of abstract and indexing annotation must be entered when the overall report is classified)

1. ORIGINATING ACTIVITY (Corporate author)	2a. REPORT SECURITY CLASSIFICATION
Naval Research Laboratory Washington, D.C. 20390	Unclassified
	2b. GROUP

3. REPORT TITLE

WIND WAVE STUDIES: PART 1, DOPPLER SPECTRA

4. DESCRIPTIVE NOTES (Type of report and inclusive dates)

This is a final report on one phase of the problem; work on other phases is continuing.

5. AUTHOR(S) (First name, middle initial, last name)

J.W. Wright, J.R. Duncan, and W.C. Keller

6. REPORT DATE	7a. TOTAL NO. OF PAGES	7b. NO. OF REFS
November 8, 1972	24	20

8a. CONTRACT OR GRANT NO.	9a. ORIGINATOR'S REPORT NUMBER(S)
NRL Prob. R07-17	
b. PROJECT NO.	NRL Report 7473
RR 021-01-41-5555	
c.	9b. OTHER REPORT NO(S) (Any other numbers that may be assigned this report)
d.	

10. DISTRIBUTION STATEMENT

Approved for public release; distribution unlimited.

11. SUPPLEMENTARY NOTES	12. SPONSORING MILITARY ACTIVITY
	Department of the Navy (Office of Naval Research) Arlington, Virginia 22217

13. ABSTRACT

Previous measurements of doppler spectra in microwave backscattering in a wind wave tank at 9.375 and 23.9 GHz have been extended to 70.1 GHz at a 3-m fetch and to longer fetches and higher winds at the lower microwave frequencies. The development of the doppler spectra with fetch and windspeed leads to the identification of three scattering wave systems. At high angles, the dominant wind waves are the dominant scatterers; the scatterers at the lower angles comprise wave systems which are respectively bound to and free of the dominant wave. The free waves are treated as a perturbation of the wind drift, and the relation of free-wave growth to the wave-breaking process is discussed.

14. KEY WORDS	LINK A		LINK B		LINK C	
	ROLE	WT	ROLE	WT	ROLE	WT
Dominant wind wave						
Wave systems, free and bound to dominant wave						
Doppler bandwidth						
Doppler spectra						
Bragg scattering						
Microwave Scattering						

CONTENTS

ABSTRACT

Previous measurements of doppler spectra in microwave backscattering in a wind wave tank at 9.375 and 23.9 GHz have been extended to 70.1 GHz at a 3-m fetch and to longer fetches and higher winds at the lower microwave frequencies. The development of the doppler spectra with fetch and windspeed leads to the identification of three scattering wave systems. At high angles, the dominant wind waves are the dominant scatterers; the scatterers at the lower angles comprise wave systems which are respectively bound to and free of the dominant wave. The free waves are treated as a perturbation of the wind drift, and the relation of free-wave growth to the wave-breaking process is discussed.

PROBLEM STATUS

This is a final report on one phase of the problem; work on other phases is continuing.

AUTHORIZATION

NRL Problem R07-17
Project RR 021-01-41-5555

Manuscript submitted August 2, 1972.

WIND WAVE STUDIES

PART 1, DOPPLER SPECTRA

INTRODUCTION

The decomposition of the variance γ^2 of the surface displacements of a wind wave system into contributions from elementary regions of wavenumber and frequency may be designated the complete spectrum of the wind wave system. Under such a decomposition the system is described by the transform pair

$$Z(\bar{r}, \tau) = \int_{-\infty}^{\infty}\int \Psi(\bar{k}, \omega) \cos(k \cdot r - \omega\tau)\, d\bar{k}\, d\omega$$

$$\Psi(\bar{k}, \omega) = (2\pi)^3 \int_{-\infty}^{\infty}\int Z(\bar{r}, \tau) \cos(k \cdot r - \omega\tau)\, d\bar{r}\, d\tau \tag{1}$$

where

$$Z(0, 0) = \overline{\gamma^2}$$

$$\Psi(-k, -\omega) = \Psi(k, \omega)$$

and we assume an implicit dependence on windspeed, fetch, air-water temperature difference, and such other intensive variables as may determine the state of the disturbed water surface. Wright (1) suggests that doppler spectra in microwave scattering by wind waves be interpreted in terms of these complete spectra. In fact in certain theoretical treatments, as will be discussed in more detail in the third section, the two spectra are proportional. That is, the backscattered power spectral density $P(k_0, \theta, \omega)$ obeys the relationship

$$P(k_0, \theta, \omega) = g(\theta)\, \Psi(2k_0 \cos\theta, 0, \omega), \tag{2}$$

where k_0 is the microwavenumber, θ the depression angle, $2k_0 \cos\theta$ the Bragg wavenumber, the water wave vector has been expressed in Cartesian coordinates k_x, k_y (see Fig. 1), and $g(\theta)$ depends also on polarization and dielectric constant.

Theoretical considerations aside, the wind wave tank scattering measurements of Wright and Keller (2) at a fetch of 3 m yielded doppler bandwidths, mean frequency shifts, and total backscattered powers which could be empirically characterized largely as functions of Bragg wavenumber rather than microwavenumber and depression angle separately. We have now extended these measurements to 70.1 GHz and also to longer fetches and higher winds in the new facility described in the next section. The development of these spectra with increasing fetch and windspeed is described in the third section, and leads to the identification of scattering from three sources: the dominant wind wave, a small-scale structure bound to the dominant wave, and a small-scale wave system

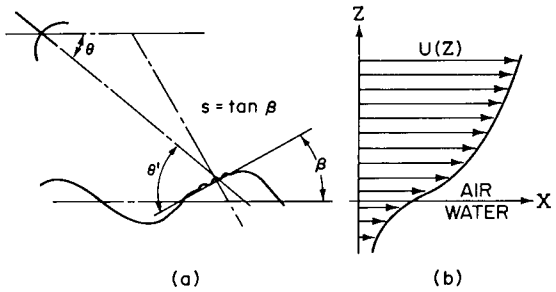

Fig. 1 — (a) Scattering geometry
(b) Shear flow profile

relatively free of the dominant wave. The mean wave speed, i.e. the quotient $\overline{\omega}/2k_0 \cos\theta$, where

$$\overline{\omega} = \frac{\int_{-\infty}^{\infty} \omega P\,(k_0, \theta, \omega)\, d\omega}{\int_{-\infty}^{\infty} P\,(k_0, \theta, \omega)\, d\omega} \tag{3}$$

of the free wave system proves to be relatively fetch independent and we follow up our previous suggestion (2) that these waves be interpreted as perturbations of the wind drift with the Orr-Sommerfeld calculation of the fourth section. As the comparison between calculated and measured phase speeds is successful, inferences drawn from visual observations in the tank are added to construct, in the fifth section, a more qualitative but possibly more accurate picture of short-wavelength wind waves than is available from first-order perturbation theory. Topics discussed include the relation of the Orr-Sommerfeld singularity with wavebreaking and the interaction of long and short waves. Finally the conclusions are more formally and concisely stated in the last section.

EXPERIMENTAL FACILITIES AND EQUIPMENT

A minority of the measurements reported here were made in the small wave tank previously described in Ref. 2. The remainder were made in a new wave tank facility, much larger than but functionally similar to the smaller tank, and the description given here is limited to the features of tank and equipment which differ substantially from the smaller installation.

The new tank is 18 m long and 1.2 m wide. The water depth is 30 cm and the wind tunnel height the same. A centrifugal blower powered by a 15-hp motor provides winds up to 20 m/s. The tank is located in a large warehouse building. Most of the measurements were made during July and August when the water temperature was between 22°C and 26°C. Cox (3) reported that neither ambient temperature nor humidity had any discernible effect on the rms slope of wind waves in his tank, but unstable thermal conditions are known to affect the wind profile (4) and may affect the surface structure.

Consequently we monitored the air-water temperature difference and found that the air temperature at the fan inlet was always 1°C to 5°C warmer than the water, corresponding to neutral or stable conditions. Fetch variation is accomplished by adding or removing roof sections of the wind tunnel. The measurements are made 1.2 m downwind of the open end of the wind tunnel and expansion of the airstream leads to a decremental upwind-downwind gradient in the wind of about 5% per meter. The mean windspeed at the maximum in the vertical profile midway between the tank walls was measured with an Alnor Velometer and is given as the single, nominal, measure of the windfield. The calibration of the velometer was found to be accurate when checked against a United Sensors pitot static tube coupled to a Dynasciences Model P109D transducer, which combination we had in turn calibrated absolutely by rotation. The wind tunnel heights in the two tanks differed so the windfields are best compared via the mean surface drift, which was 4.6% of the nominal or reference wind in the small tank and 3.5% in the large tank. Windspeeds from the small tank are reported in this paper multiplied by the ratio 4.6/3.5, but measurements made in the small tank are always so identified. Note that, due to a numerical error, the reference windspeeds reported in Ref. 2 are too large and should be multiplied by 0.91. Comparison of the winds in our tank with other tanks or the ocean may be made in terms of the friction velocity μ_a^*. Following Shemdin and Lai (5), we write the velocities in the water and air (see Fig. 16 of Ref. 5).

$$U_a(Z) = U_s + \frac{\mu_a^*}{\kappa} \ln \frac{Z + Z_0^a}{Z_0^a} \tag{4a}$$

$$U_w(Z) = U_s + \frac{\mu_w^*}{\kappa} \ln \frac{Z + Z_0^w}{Z_0^w} \tag{4b}$$

where

μ^* = friction velocity

κ = Karmans constant

Z_0 = so-called roughness length

and a, w, and s refer to air, water, and surface, respectively. We measured drift profiles as described in Ref. 2 for winds up to 7 m/s in addition to these reported previously which extend to an equivalent large tank windspeed of 9.3 m/s. Our values of μ_w^* and Z_0^w are compared with these of Shemdin and Lai in Table 1. The agreement is quite satisfactory. If we assume continuity of the mean shear stress at the surface, then

$$\rho_a (\mu_a^*)^2 = \rho_w (\mu_w^*)^2, \tag{5}$$

where ρ is density and μ_a^* may be obtained from μ_w^*. In Fig. 2 we have plotted these calculated values of μ_a^* together with friction velocities taken from Fig. 15 of Shemdin (6), from Kunishi (7) and from Hidy and Plate (8). By fitting our measured profiles to Eq. (4b) and using Eq. (5) we obtained

$$\mu_a^* = 0.046\ W, \tag{6}$$

Table 1
Wind Drift Profile Parameters

U_s (cm/s)	μ_w^*/κ (cm/s)		z_0^w (cm)	
	Wright & Keller†	Shemdin & Lai‡	Wright & Keller†	Shemdin & Lai‡
8.5	—	0.9	—	0.04
10	1.5	—	0.016	—
14	2.0	—	0.009	—
15	—	2.2	—	0.04
19	2.6	—	0.009	—
26	2.6	—	0.008	—
27	—	3.2	—	0.02
33	3.9	—	0.010	—

†Ref. 2
‡Ref. 5

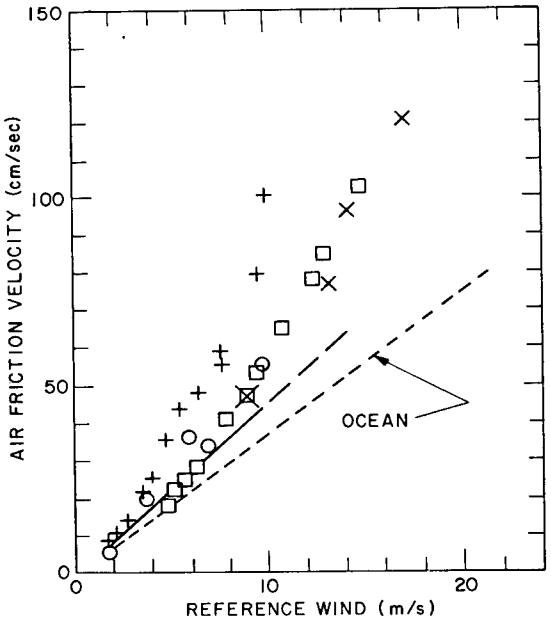

Fig. 2 — Air friction velocitics as a function of reference wind for several wave tanks and the ocean. ○ — Shemdin (6); + Kunishi (7); □ — Hidy and Plate (8); X — this report.

where W is the reference wind. This is the solid and dashed line in Fig. 2. Since the measurements from others' tanks deviate from this line at the higher winds, we made some determinations of μ_a^* from measurements of the wind profile. These are also given in Fig. 2. The ratio $(\mu_a^*/w)^2$ is the drag coefficient, and taking a value 1.5×10^{-3} as representative of the ocean yields the dotted line in Fig. 2. However, some observers have reported that the drag coefficient over the ocean increases with increasing wind (9). Caution is urged in using Fig. 2 for quantitative transformation of wave tank data to the ocean. Obviously the dominant wave and the wave-breaking process are much different in the tank than they are at sea.

If it is assumed that each 30-s average taken by the doppler spectrometer is an independent sample and further that the rms statistical error ϵ in this average is independent of frequency, then it is straightforward to estimate the statistical error in the mean frequency shift and doppler bandwidth. Measurements of ϵ in a few representative cases yielded a value 0.15 which agrees well with that calculated from the filter bandwidth B, and integration time T according to the relation $\epsilon \approx (BT)^{-1/2}$. The statistical error in mean frequency shift was calculated to be 2 to 4% of the bandwidth and was usually smaller than systematic spectrometer errors, to which a value equal one-half the frequency interval corresponding to an integration time has been assigned. The statistical error in the bandwidth was in the range 2 to 20%.

The audio and microwave equipment is mounted on a truck which spans the tank and rolls on tracks to allow ready changes in fetch. The instrumentation is similar to that described in Ref. 2 except that the use of parabolic antennas has largely eliminated the spectral broadening introduced by the Fresnel zone structure. We have used monochromatic, mechanically generated water waves to measure the antenna function $V(k_x, k_y)$ which, according to a slight generalization of Eq. (4) of Ref. 2 is convolved with the surface displacement spectrum to give the scattering cross-section σ°

$$\sigma^0 = 16\pi k_0^4 gg^* \int_{-\infty}^{\infty}\int \psi\,(k'_z, k'_y\,\omega) \tag{7}$$

$$V\,(2k_0\,\cos\theta - k'_z, k'_y)\,dk'_z, dk'_y.$$

These antenna measurements will be reported in detail elsewhere but $V(k_x, k_y)$ for the parabolas used in these measurements as well as for the horn previously used at 23.9 GHz are shown in Fig. 3. Finally, we will henceforth denote 9.375 GHz as X-band, 23.9 GHz as K-band and 70.1 GHz as V-band. The notation $K\ 30^\circ VV$, e.g., then denotes 23.9 GHz, a depression angle of 30°, and vertical polarization on transmission, vertical polarization on reception.

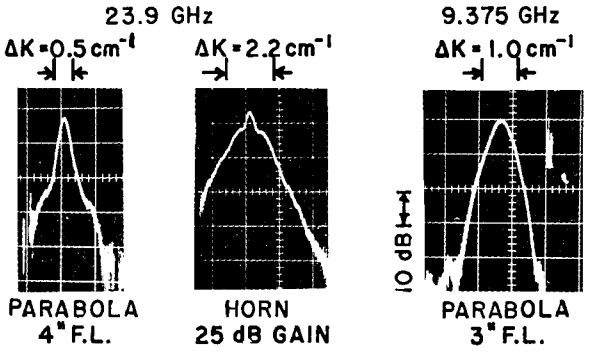

Fig. 3 — Fourier transforms of antenna patterns. The vertical scale is 10 dB/large division in each case. The horizontal scales vary. The width of the pattern 12 dB below the peak, ΔK, is given in each case. The abbreviation F.L. means focal length.

WINDSPEED AND FETCH DEPENDENCE OF DOPPLER SPECTRA

A feature of most wind wave systems is the existence of distinct scales of roughness. On the open ocean there may be several scales such as swell, dominant wind wave, "equilibrium" range gravity wave, etc. In a laboratory wind wave tank, however, the situation is simpler and there is an evident dichotomy between the larger scale dominant wind wave and a smaller scale structure. This dichotomy provides an intuitive basis for the application of a composite surface scattering model. Several such models exist (see references cited in Ref. 2). All suffer the drawback that the division into large- and small-scale structures is arbitrary and none treat doppler spectra quite adequately. Hence it is simpler to develop the required characteristics of such a composite surface model from the measured spectra rather than to review several theories, none of which are quite matched to our measurements.

At a sufficently low wind and short fetch the entire wind wave system is small scale. In a case, shown in Fig. 4, where the rms surface displacement is a millimeter or less, the mean frequency shifts and bandwidths of doppler spectra taken at 9.375 and 23.9 GHz, respectively, at depression angles yielding identical Bragg wavenumbers, are very similar. This fact and the result, not shown, that the scattering cross section with horizontal polarization is 15 dB less than that with vertical polarization at the lower angle, are characteristic of scattering describable by perturbation theory, i.e. of scattered fields (nearly) proportional to surface displacement. We call this type of scattering low-order Bragg scattering. If the surface displacement were describable as a linear superposition of free, horizontally traveling waves, all so small that the net particle motion were negligible compared to the component wave phase speeds, there would be no spectral broadening. In fact an outstanding characteristic of our previous measurement (2) at a fetch of 3 m was the broadening of the rms bandwidth $\Delta\omega$ with increasing wind according to the relation

$$\Delta\omega = \omega_0 + 2\, k_0\, V_0 \cos\theta, \tag{8}$$

where

$$(\Delta\omega)^2 = \frac{\int_{-\infty}^{\infty} (\omega - \bar{\omega})^2\, P(k_0, \theta, \omega)\, d\omega}{\int_{-\infty}^{\infty} P(k_0, \theta, \omega)\, d\omega} \tag{9}$$

and V_0 is an empirically determined velocity. The same relation has now been found to hold at 70.1 GHz at the 3-m fetch in the small tank as can be seen in Fig. 5a. Bandwidths measured at 23.9 GHz at a fetch of 12 m and a windspeed of 15 m/s also yield a proportionality to Bragg wavenumber as can be seen in Fig. 5b. The deviations from this proportionality occur at depression angles of 70° and greater, where the scattering mechanism may be other than Bragg scattering.

The simplest way in which doppler broadening can be obtained is to relax the requirement that the net particle velocity be very small compared to component phase speeds. Consider, then, advection of small waves by large waves, neglecting, however, the influence of the large wave motions on the small wave amplitude. The doppler bandwidth due to

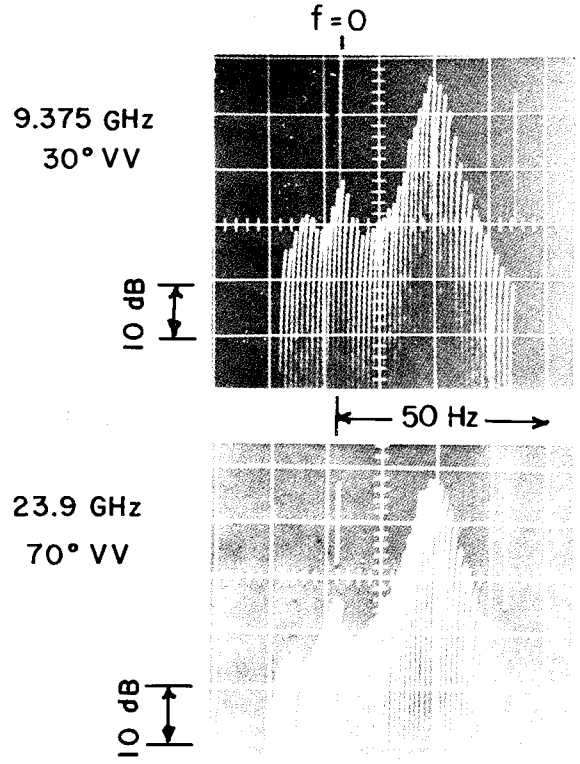

Fig. 4 — Doppler spectra in Bragg scattering. Windspeed = 3.5 m/s, fetch = 2.75 m, $2k_0 \cos\theta = 3.4$ cm^{-1}.

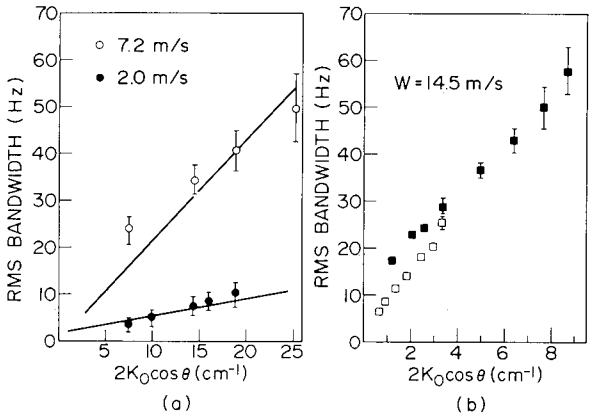

Fig. 5 — Doppler bandwidth on vertical polarization (a) 70.1 GHz, fetch = 3m, small tank. The solid lines are from Ref. 2, Fig. 7 (b) ■ 23.9 GHz, □ 9.375 GHz, fetch = 12 m, large tank.

advection can then be determined in the following way. Suppose C_c is the phase speed of the dominant wave and C the phase speed of the small wave obtained from solution of the appropriate hydrodynamic boundary value problem solved in the frame moving at the local particle velocity, assumed locally uniform. If u and w are the horizontal and vertical components of large wave orbital velocity, s the large wave slope, θ the depression angle, and θ' the depression angle relative to the large wave slope (see Fig. 1), then the projection of the small wave speed along the line of sight is $u\cos\theta + C\cos\theta' + w\sin\theta$. To first order in large wave slope,

$$\cos\theta' = \cos\theta - s\sin\theta$$

$$w = C_c s,$$

so the doppler shift ω is

$$\omega = 2k_0 \left[(u + c)\cos\theta + (C_c - C)\, S\sin\theta\right]. \tag{10}$$

Since $\bar{u} = \bar{s} = 0$ the mean doppler shift is $2k_0 C\cos\theta$, which is, of course, the frequency of the first-order Bragg wave. The rms doppler bandwidth $\Delta\omega$ is then

$$\Delta\omega/2k_0 = \left[\bar{u}^2 \cos^2\theta + \overline{us}\,(C_c - C)\sin 2\theta + (Cc - C)^2\,\bar{s}^2 \sin^2\theta\right]^{1/2}. \tag{11}$$

In first order $\overline{us} = 0$, and as, particularly at short fetch, the crest and mean phase speeds prove to be nearly equal, Eq. (11) yields the observed dependence of doppler bandwidth on Bragg wavenumber. However, the value of orbital velocity required is much too large, the ratio of V_0 to crest speed reaching 0.4 at a windspeed of 15 m/s and a fetch of 12 m. The reason for this can be discerned in Fig. 6; there is another contribution to the bandwidth which is a very substantial fraction of the whole at the higher winds. This is evident from the fact that the bandwidths in Fig. 6 do not vanish at very short fetch, which they would were they due to orbital velocity alone.

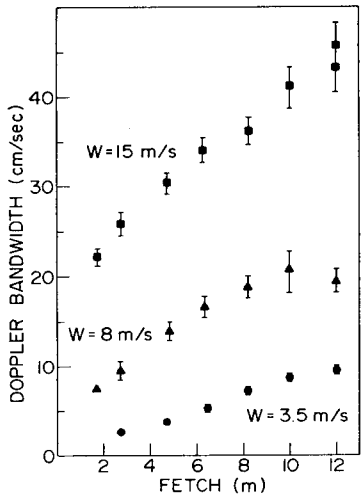

Fig. 6 — Doppler bandwidth in velocity units, $\Delta\omega / 2k_0 \cos\theta$, as a function of fetch. ■ 23.9 GHz, 50° VV; ▲ 9.375 GHz, 30° VV; ● 9.375 GHz, 30° VV.

Although orbital velocity is not the only contributer to spectral broadening, theoretical interpretations of doppler spectra based on advective motions of first-order Bragg waves are useful in understanding the measurements. Thus in the analogous problem of first-order, scalar, volume scattering by density fluctuations in a fluid, Ford and Meecham (10) have deduced that the proportionality of Eq. (2) is retained and the doppler spectrum, appropriately normalized and in the absence of correlation of scatterer strength with advecting velocities, is the probability distribution of advecting velocities parallel to the Bragg wave vector. Hasselmann and Schieler (11) have treated the immediately relevant problem of scattering from the ocean, taking into account correlation of scatterer strength with both large wave slope and particle motions. Unfortunately our inability to isolate the effects of orbital velocity, and some other complications discussed shortly, make it difficult to compare our measurements quantitatively with their results.

Spectra taken at high angles are characteristically sharply peaked, triangular appearing, and asymmetric, as can be seen in Fig. 7. The very close correlation of the quotient of the peak angular frequency by Bragg wavenumber with crest speed over a wide range of the two independent variables, fetch and windspeed, as shown in Fig. 8, clearly associates the high-angle scatter with the dominant wave. Scatterers moving at velocities near the crest speed are also evident in some cases at lower angles. This is illustrated in Fig. 9, which shows spectra taken with both horizontal and vertical polarization at a windspeed of 15 m/sec, fetch of 12 m, depression angle of 30°, and at 9.375 GHz. We interpret the absence on horizontal polarization of the broad spectral peak present on vertical polarization to be the polarization signature of low-order Bragg backscatter, as previously discussed. A second scattering phenomenon is evident which is relatively polarization independent and more sharply peaked, the peak occurring at a doppler speed of about 98 cm/sec compared to the measured crest speed of 117 cm/sec. It is interesting to note that polarization ratios near unity are also observed at sea at X band, with lower angles and higher winds, a phenomenon which is not readily explainable by the usual composite surface theories. Thus the phenomenon observed here may be at the root of observations of unity polarization ratio at sea.

Scatterers moving at or near the crest speed, though not necessarily exhibiting polarization independence, are also observed at lower winds and shorter fetches. A particularly vivid illustration of this is shown in Fig. 10a. At 30° and 23.9 GHz the Bragg resonant wavelength is about 7mm, which is a parasitic capillary wavelength. Thus at a windspeed of 5 m/sec and very short fetch the peak frequency of the doppler spectra corresponds almost exactly with the crest speed. The correspondence is maintained at intermediate fetch, but at the longest fetch the crest speed is too great for the parasitic wave system which breaks away from the dominant wave as is indicated by a peak doppler shift which, if anything, is slightly less than at the intermediate fetch. The peak frequency does not return to the value at the shortest fetches, however, showing that the small waves are not completely free of the large wave. This can be understood in another way following the ideas of Hasselmann and Schieler (11). At these moderate winds the small waves exist only in the region forward of the large wave crests where the horizontal component of large wave orbital velocity is large and downwind. The mean speed of the small wave is thus increased by the mean value of the horizontal particle velocity in the region where the small waves exist. Some waves or surface irregularities do remain bound to the crest, however, and scattering from these contributes the asymmetry to the spectrum at the long fetch.

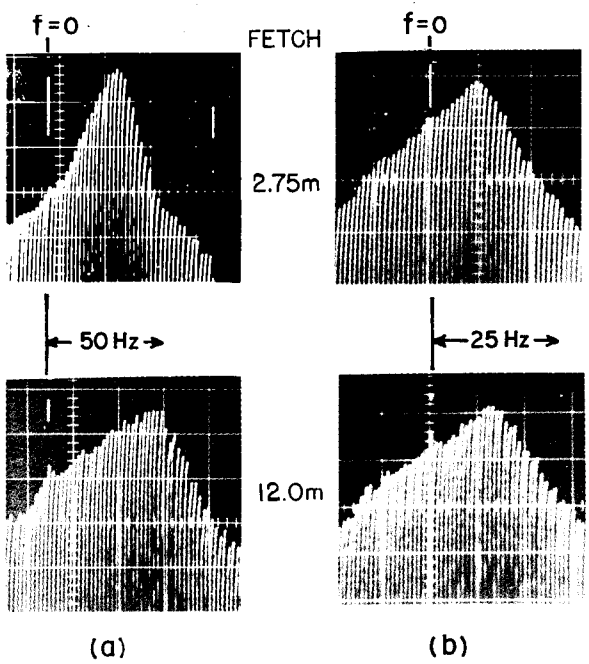

Fig. 7 — Doppler spectra at high angles. (a) 23.9 GHz, 70° VV, windspeed = 8 m/s, (b) 9.375 GHz; 80° VV, windspeed = 15 m/s

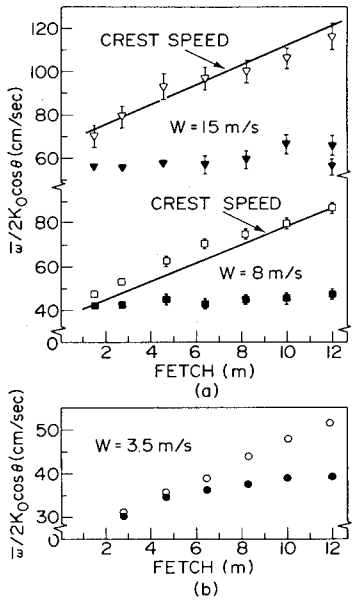

Fig. 8 — Fetch and windspeed dependence of mean wave speeds. (a) ▽ 9.375 GHz, 80° VV; ▼ 23.9 GHz, 50° VV; □ 23.9 GHz, 70° VV; ■ 9.375 GHz, 30° VV. The solid lines are least mean squares linear fits to the measured crest speeds, (b) ○ 23.9 GHz, 70° VV; ● 9.375 GHz, 30° VV.

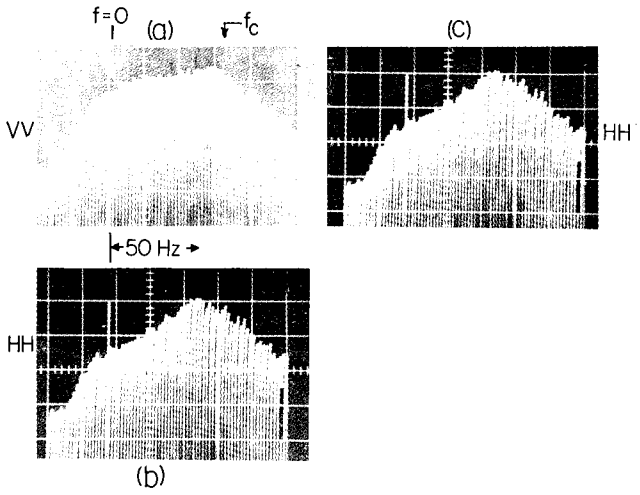

Fig. 9 — Doppler spectra at 9.375 GHz, 30° on vertical and horizontal polarization. b and c are identical spectra. The amplitude scales for a and b are in register.

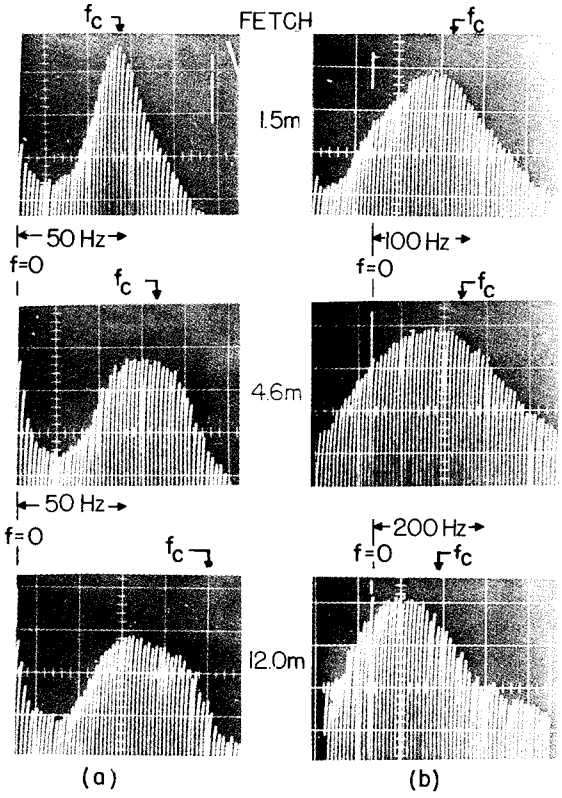

Fig. 10 — Development of doppler spectra with fetch. Vertical scale = 10 dB per large division, $2\pi f_c = 2k_0 C_c \cos\theta$. (a) 23.9 GHz, 30° VV, windspeed = 5 m/s, (b) 23.9 GHz, 50° VV, windspeed = 15 m/s.

At high winds the crest speed is too great for the existence of a parasitic wave system even at the shortest fetch. At 15 m/s rudiments of the scattering phenomenon discussed in connection with Fig. 9 were often evident, but at 23.9 GHz and 50°, in the case shown in Fig. 8b, relatively symmetrical doppler spectra with mean frequency nearly independent of fetch are observed. Fetch and windspeed dependencies of mean or peak doppler shifts are summarized in Fig. 8. The mean wave speed (Eq. (3)) is given for the spectra taken at 30° and 50° but in the case of the characteristically asymmetric and sharply peaked high-angle spectra it is more natural to use the peak frequency, the close correlation of which with the crest speed has already been noted. The weak dependence on fetch crest at the lower angles is attributable to bound waves or other scatterers moving near the speed. Many of the lower windspeed spectra exhibit a shallow bifurcation which delineates the separate contributions of relatively free and relatively bound waves. The series of measurements at 15 m/s, 23.9 GHz, and 50° in Fig. 8 was made a few days after the spectrum at 12 m shown in Fig. 8b was taken. Visual inspection of the spectrum corresponding to the mean wave speed at 12 m in Fig. 8 makes it clear that the increase in mean wave speed over that at the shorter fetches is due to the presence of scatterers, which are absent in the spectra of Fig. 10b, moving at nearly the crest speed. Further evidence of the influence of a factor other than fetch or windspeed on the crest-bound scatterers is discussed in the next section.

For winds less than 5 m/s, polarization ratios $\sigma^0_{vv}/\sigma^0_{hh}$ of 10 dB or greater at 9.375 GHz and 30° are observed at all fetches and this can be accounted for on the basis of composite surface theory using first-order Bragg scattering and a mean tilt of about 10°. The trend toward unity polarization ratio at high winds is largely due to scatterers moving at or near the crest speed. In many cases, it is possible to estimate the scattered power due to the bound and free wave systems separately. The minimum polarization ratios observed for the free waves at 30° and all winds and fetches are 6 to 8 dB. Such ratios may be obtained formally from the composite theory using first-order Bragg scattering. However, a rational means of dividing the surface into long and short waves, such as may be provided by our high-angle measurements, together with simultaneous measurement of wave slopes and polarization ratios, is required to quantitatively determine whether the first-order theory is entirely adequate.

WAVES WHICH EVOLVE FROM WIND DRIFT

The simplest waves of the three types we have abstracted from the overall wind wave system are the free waves. Visual observation makes it clear that these free waves are, roughly, short gravity and capillary waves, but they differ from the classical water wave since the wave speed depends markedly on the wind. The fact that this speed is also relatively fetch independent immediately suggests the influence of wind drift, the highly sheared flow at the air — water interface, which is known to possess the same property (12,13). Thus we are led to treat the free wave system as a perturbation of the wind drift. The perturbation of a shear flow is an Orr-Sommerfeld problem, and the flows with which we deal are the coupled mean shear flows in the air and water. The calculation in the air is the basis of Miles' well-known theory of wind wave generation (14), but Miles assumed the phase speed to be given rather than obtaining it as an eigenvalue of the hydrodynamic boundary value problem.

If $w(x, z)$ is the vertical component of perturbed velocity, the Rayleigh equation (15) is

$$\frac{d^2w}{dz^2} - \left(k^2 + \frac{U''}{U - C}\right)w = 0, \tag{12}$$

where k is the wavenumber, U the mean shear flow assumed to depend only on z, and C the phase speed of the harmonic perturbation. Equation (10) can be put into a form convenient for numerical integration by use of the substitution $y = w^{-1}\, dw/dz$. Then we integrate to the surface from great heights above in the air and great depths below in the water:

$$y_a^0 = k + \int_{\infty}^{0} \left[\left(k^2 - y_a^2\right) + \frac{U''}{U - C}\right] dz \tag{13}$$

$$y_w^0 = k + \int_{-\infty}^{0} \left[\left(k^2 - y_w^2\right) + \frac{U''}{U - C}\right] dz. \tag{14}$$

The two quantities are related by the first-order boundary conditions obtained by expanding velocity and pressure fields in Taylor series, equating normal stresses, and applying the kinematic boundary condition, all in the usual way:

$$y_w^0 - \left(\frac{\rho_a}{\rho_w}\right) y_a^0 = \frac{U_s'}{(U_s - C)} \left[1 - \left(\frac{\rho_a}{\rho_w}\right)^{1/2} \left(\frac{z_w^0}{z_a^0}\right)\right] + \frac{kC_0{}^2}{(U_s - C)^2}. \tag{15}$$

The logarithmic profiles, Eqs. (4a) and (4b), have been used,

$$U_s' \equiv u_w^*/(\kappa z_0^w), \tag{16}$$

and C_0 is the phase speed for infinitesimal waves in the absence of wind,

$$C_0 = \sqrt{\frac{g}{k} + Sk}, \tag{17}$$

where g is the acceleration of gravity and S the ratio of surface tension to water density.

For the gravity waves with which he was largely concerned, Miles (14) found that the effect of the shear flow on the air was to make relatively small changes in the complex water wave propagation constants. In the case of gravity waves for which

$$k^{-1} >> L \equiv \frac{U_s}{U_s'} = \frac{U_s z_0^w}{u_w^*/\kappa} \approx 1 \text{ mm}, \tag{18}$$

the effect of the shear flow in the water will also be small, for then the particle motions of the wave go deep compared to those of the wind drift. In that case it is necessary to solve the full coupled problem. In the case of our scattering measurements, however, the Bragg wavenumbers are of order $1/L$. In this case the shear flow in the water is more important, and we expect that the contributions to Eq. (3) from the air will be of order $y_w^0 \sqrt{\rho_a/\rho_w}$. To retain some measure of the coupling we reverse Miles' procedure. That is, we use Miles' uncoupled formulation in the air to estimate the effect on the phase speed of the component of air pressure in phase with the perturbed displacement. Then, neglecting terms of order $\sqrt{\rho_a/\rho_w}$, Eq. (15) becomes

$$y_w^0 = \frac{U_s'}{(U_s - C)} + \frac{k\,[C_0^2 + \alpha\,(u_w^*/\kappa)^2]}{(U_s - C)^2}, \tag{19}$$

where α is the parameter defined by Miles (14), in his Eq. (2.3). For values of C/u_a^* as small as those characteristic of the present problem, Miles (16,17) considered it necessary to take the viscous sublayer into account but did not carry the problem as far as calculating values of α. As the details and even the existence of such sublayers are uncertain and the value of α is not crucial in the present context, it is expedient to leave α as an adjustable parameter. Values of C, calculated by simultaneous numerical solution of Eqs. (14) and (19), using the profile of Eq. (4b) are given for several values of z_0^w and α in Table 2.

Table 2
Calculated Phase Speeds for k = 3.4 cm^{-1}

Surface Drift U_s (cm/s)	$\overline{C} - U_s$ (cm/s)		
	z_0^w = 0.02 cm, α = 0	z_0^w = 0.01 cm, α = −10	$z_0^w = 0.3/U_s$ cm, α = 0
0	23.3	23.3	23.3
10	20.1	19.6	—
20	17.4	15.3	17.1
30	15.0	11.0	14.5
40	12.8	6.2	11.9
45	—	4.2	10.4
47.5	—	3.4	—
50	11.0	2.5	8.6
52.5	—	2.1	—
55.0	10.0	1.7	7.1

To compare the calculated phase speeds with mean wave speeds we measured a series of doppler spectra at short fetch, at 9.375 GHz, 30° on both vertical and horizontal polarization and concurrently measured the surface drift with small floats. This choice of fetch, depression angle, and microwavelength yielded polarization ratios greater than 10 dB in all but three cases where it was 8 dB, thus assuring that we were viewing low-order Bragg scatter, while also permitting measurement of float speeds to higher winds before the floats were plunged below the surface by breaking waves. The results of these measurements are compared with calculated phase speeds in Fig. 11. Since many of the measurements were made at a fetch of 1 m where the surface drift was a somewhat lesser fraction of the wind at lower windspeeds, the mean surface drift is used as the independent variable in Fig. 11. The horizontal bars on the data points in Fig. 11 have a length of twice the standard deviation in a series of 15 consecutive measurements, and the windspeed scale at the top of the graph gives the wind which corresponds approximately to the surface drift. Even at the shortest fetch we were unable to obtain reliable measurements of float speed for speeds in excess of 40 cm/s (winds greater than 11.5 m/s) and the drift speeds for higher winds were extrapolated from the float speed measurements for winds less than 11.5 m/s. Despite the unavoidably large uncertainty in the drift speeds, the possibility of an Orr-Sommerfeld singularity (vanishing of $\overline{C} - \overline{U}_s$) is clearly indicated by the data of Fig. 9. Values of $z_0^w = 0.01$ cm and $\alpha = -10$, which represent a fairly strong coupling to the air, provide a significantly better fit than $z_0^w = 0.02$ cm, $\alpha = 0$.

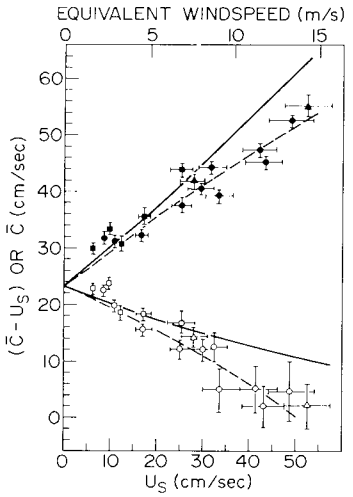

Fig. 11 — Comparison of mean wave speeds, $\overline{C} = \overline{\omega}/2k_0 \cos\theta$, measured at 9.375 GHz, 30° VV, with phase speeds calculated from the first-order Orr-Sommerfeld equation. Open data points are $\overline{C} - U_s$, solid points $\overline{C}$. ○, ● — fetch = 1 m. □, ■ fetch = 2.75 m. Δ, ▲ — all fetches. Solid line is for $z_0^w = 0.02$ cm, $\alpha = 0$: dashed line $z_0^w = 0.01$ cm, $\alpha = -10$.

Interestingly enough the bandwidth at 9.375 GHz, 30°VV, and 1 m fetch increases rapidly at the higher winds as is shown in Fig. 12. The square data points are all taken from Fig. 4, the 23.9-GHz bandwidths at 15 m/s having been converted to 9.375-GHz bandwidths, assuming proportionality with Bragg wavenumber, as was indeed found at the longest fetch. The solid line is calculated from $V_0(W)$ given in Ref. 2, Fig. 8, and plotted by converting small tank windspeeds to equivalent large tank winds by multiplying by the ratio of surface drifts. The rapid increase in bandwidth may be due to short wave growth associated with the Orr-Sommerfeld singularity. Temporal and/or spatial fluctuations in the mean drift are another possible cause.

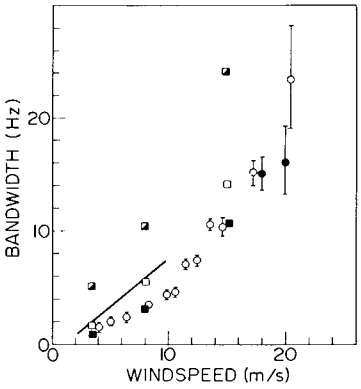

Fig. 12 — Dependence of bandwidth on windspeed at 9.375 GHz, 30° VV. The solid line is taken from Ref. 2, Fig. 8, The square data points are from Fig. 4. ○, ● — fetch = 1 m; □ fetch = 1 m, □ fetch = 3.1 m, ◪ fetch = 12 m.

There are indications in some of the spectra taken at the short fetches that the rapid increase in bandwidth at the high winds is due to blooming of the spectrum about the crest speed rather than about the mean wave speed. In addition, the magnitude of the bandwidth at 1-m fetch and 15 m/s is very nearly the same as the bandwidth of the spectra on horizontal polarization shown in Fig. 9. This suggested that the two phenomena might be connected. We measured a series of spectra at 9.375 GHz, 30° HH, at 15 m/s and found that the bandwidth was indeed independent of fetch and twice as large as that in Fig. 9 which had been measured a few months before! An attempt to fill in the data of Fig. 12 at high winds at a later date yielded similar differences in bandwidth as is indicated by the solid circular data points in Fig. 12. It is thus very clear that a factor other than fetch or windspeed is operative at the higher winds. Because we monitored the difference between the water temperature and the air temperature near the fan inlet, we know that there were no cases of marked thermal instability. Nonetheless a systematic study of the effect of air — water temperature differences on the doppler spectra is clearly in order.

The wavenumber dependence of the mean wave speeds is shown in Fig. 13. Some of the data are identical with those in Ref. 2, but new data of 70.1 GHz have been added at both windspeeds. Results from the large tank at 9.375 GHz and an equal surface drift have also been added. Measurements for depression angles greater than 65° have been eliminated from Fig. 13, since the present work shows that in those cases one measures the crest speed rather than the mean free wave speed. Of course, at a fetch of 3 m there is not a great difference between the two. We believe that the independence of wavenumber exhibited by the phase speed at large wavenumbers results from the fact that these very short waves are bound to the longer waves of the free wave system. Perhaps they are, in some cases, harmonics of Crapper (18) waves. In any event we found no evidence of really free capillary waves in the millimeter region. At a windspeed of 15 m/s we also measured doppler shifts as a function of depression angle at 23.9 and 9.375 GHz at a 12-m fetch and 70.1 GHz at a 1-m fetch. These two sets of data are thus not directly comparable; in addition, at the long fetch subjective judgement is required in isolating the effect of scatterers at the crest speed. With these qualifications we can get estimates of mean free wave speed as a function of Bragg wavenumber at 15 m/s also. They lie in the range of 52 to 58 cm/s for wavenumbers between 1.9 cm^{-1} and 18 cm^{-1}. The wavenumber being independent of the mean wave speed has the interesting consequence that the interpretation of this speed does not depend on the order of the Bragg scattering, as it is only when the phase speed of Fourier component waves depends on wavenumber that the higher Bragg orders result in different frequency shifts.

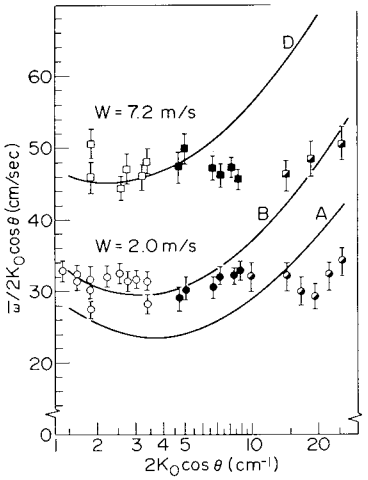

Fig. 13 — Dependence of mean wave speeds on Bragg wavenumber at fetch = 3.1 m. Open points, 9.375 GHz; solid points, 23.9 GHz; half-solid points, 70.1 GHz. Curve A is $C_0(k)$; curve B is $C(k)$ for U_s = 10 cm/sec, z_0^w = 0.01 cm, α = 0. Curve D is $C(k)$ for U_s = 33 cm/sec, z_0^w = 0.01 cm, α = 0.

Previous measurements of phase speeds of high-frequency wind waves have been reported by Cox (3) who obtained them from optical measurements of slopes in a narrow frequency band. If one assumes that Eq. (2) is indeed correct, then with minimal information about the directional properties of the spectra one can obtain Cox's correlograms by using Fourier transforms on our doppler spectra. On this basis we estimate that the quantity Cox calls phase speed should be slightly larger than our mean wave speed, though the difference is small except when the doppler spectra are quite broad. On the other hand the water depth in Cox's tank was 14 cm, half of ours, so that the surface drift, which was not measured, was probably less. Cox's measurements are given at constant frequency and ours at constant wavenumber, but the speeds are relatively independent of both. In view of these various uncertainties precise comparison is impossible, but Cox's measurements at 104 Hz are probably in satisfactory agreement with ours. He too found that the phase speed at low winds was actually less than that with no wind. At 37 Hz Cox's phase speeds are in fair agreement with ours except at the highest wind, 11.5 m/s, where he reports a significantly lower value. In the case of Cox's 6.6-Hz measurements, comparison via the Fourier transformation is impossible because such doppler shifts are observed in our measurements only at high angles where Eq. (2) is inapplicable. Nonetheless Cox's phase speeds of 31 to 32 cm/s at winds of 8.8 m/s seem inexplicably low, compared with ours. Curiously, the correlogram given in Cox's Fig. 3, which Cox considers to have too few zero crossings to permit precise determination of the phase speed, yields a phase speed of 45 to 50 cm/s which is quite in accord with our results. Only simultaneous measurements by the two methods could determine whether there is a real discrepancy between them.

THE NATURE OF WIND WAVES AT SHORT FETCH

Observation of the evolution of doppler spectra with fetch and windspeed has led to identification of three scattering wave systems. The dominant wind wave is also the dominant scatterer at high angles, and while the scattering may be describable by geometrical or physical optics methods, the spectral asymmetry and large bandwidths do not seem to be accounted for by existing formulations. The small-scale structure which is

responsible for the scattering at depression angles less than 70° is composed of wave systems which are respectively free of and bound to the dominant wave. At low winds the bound waves are the familiar parasitic capillary waves. They are not, of course, rigidly bound to the dominant wave, but move, by definition, at speeds near the crest speed. At high winds the bound waves are, perhaps, not waves in a visual sense at all, but rather the broken water ahead of the crests of the dominant waves. The free waves evolve as the bound waves break away from the dominant wave. With increasing wind their properties are increasingly determined by the wind drift with the consequence that they are rotational waves with a phase speed dependent on the wind. Just as the bound waves are not rigidly locked to the dominant wave, so the free waves are not totally unfettered but interact with the dominant wave in a number of ways.

Some of these are manifest in the development of the small-scale structure with increasing wind at the 12-m fetch in our tank. Prior to wave breaking, which under those conditions occurs at about 10 m/s, the small-scale structure is largely confined to the portion of the dominant wave leeward of the crest. At the lowest winds this is essentially the parasitic capillary phenomenon, but with increasing crest speed the effect is probably more aptly envisioned as due to the straining of the small waves by the horizontal component of orbital velocity of the dominant wave (19,20). With the approach of breaking, however, the windward side of the dominant wave, heretofore quite smooth, begins to be covered with small waves. These appear to be the free waves and at the highest winds they tend to cover the upper portions of the dominant wave quite uniformly, both leeward and windward of the crests. Since the diverging horizontal component of orbital velocity which prevents small-wave formation windward of the crests increases with dominant wave growth, the appearance of free waves on the windward slopes indicates the existence of a free-wave growth mechanism which increases more strongly with wind.

One candidate is at hand in the form of the Orr-Sommerfeld singularity, the existence of which is indicated in Fig. 9. The windspeed, W_c, at which $\overline{C} - U_s$ vanishes depends on Z_0^w and α, but also on C_0. The effective local acceleration of gravity is reduced near the crests by the centripetal acceleration of the orbital motion of the dominant wave. This reduces C_0 and in turn W_c. Thus it is near the crests that the critical layer ($C - U = 0$) first descends into the water, where it may be expected to have a larger effect because unencumbered by an unfavorable $\sqrt{\rho_a/\rho_w}$ ratio. The actual magnitude of the resulting short wave growth, unlike that of the phase speed, depends critically on the characteristics of the shear flow profile including those of the boundary layers on both sides of the air — water interface. At second order, which is probably more important in the water, the critical layer is broadened and growth will take place for winds less than W_c.

Thus, windward of the crests the straining and Orr-Sommerfeld mechanisms oppose and the resulting short wave amplitude represents a balance between the two which is tipped in favor of the former at low winds and the latter at high winds. Leeward of the crests both mechanisms promote short wave growth and the amplitude is limited by dissipation or breaking of the small waves themselves. Indeed this process may be an important part of the wave-breaking process in general. In any case it is a matter of observation that waves in tanks break at considerably higher winds than the large waves at sea. Thus wave breaking is dependent on the wind as well as on the orbital acceleration of the large waves, and the above-outlined mechanism provides a basis for that observation.

CONCLUSIONS

As a result of the investigations reported in this paper we have demonstrated the utility of microwave scattering for studying wind-generated waves in wave tanks and of low-order Bragg scattering theory in interpreting these measurements. We have shown that the small-scale structure is comprised of scatterers which are respectively free of and bound to the dominant wave. The free scatterers can be described as a wave system with a phase speed which can be calculated from a first-order perturbation of the wind drift. We have found that there is a significant contribution to the doppler bandwidth other than orbital velocity. Observations made so far are consistent with rapid small-wave growth and/or fluctuations in the surface drift as origins of this additional bandwidth.

ACKNOWLEDGMENTS

During the course of this work we benefited greatly from a number of stimulating interchanges with Prof. Omar Shemdin and the perceptive comments of Dr. Klaus Hasselmann. It is a pleasure to acknowledge those debts. We were also the fortunate recipients of excellent technical assistance from Oliver Larison and Peter Mah.

REFERENCES

1. J.W. Wright, IEEE Trans. Antennas and Propagation, **16** 217 (1968).
2. J.W. Wright and W.C. Keller, Phys Fluids, **14** 466 (1971).
3. C.S. Cox, J. Mar Res., **16** 199 (1958).
4. V.J. Cardone, Dept. of Meteorology and Oceanography, Geophysical Sciences Laboratory, TR-69-1 New York Univ. (1969).
5. O. Shemdin and R.J. Lai, "Laboratory Investigation of Wave-Induced Motion Above Air-Sea Interface," Technical Report #6, Dept. of Coastal and Oceanographic Engineering, Univ. of Florida (1970).
6. O. Shemdin, "Instantaneous Velocity and Pressure Measurements Above Propagating Waves," Technical Report #4, Dept. of Coastal and Oceanographic Engineering, Univ. of Florida (1969).
7. H. Kunishi, Bulletin #6, Disaster Prevention Research Institute, Kyoto University (1963.)
8. G.M. Hidy and E.J. Plate, J. Fluid Mech, **26** Pt 4 631 (1966).
9. O.M. Phillips, *The Dynamics of the Upper Ocean*, Cambridge University Press, London, 1966, p. 144.
10. G.W. Ford and W.C. Meecham, J. Acoust. Soc. Amer. **32**, 1668 (1960).
11. K. Hasselmann and M. Schieler, Eighth Symposium on Naval Hydrodynamics, 1970, ACR-179, Office of Naval Research, Washington, D.C., pp. 361-388.
12. G.H. Keulegan, J. Res. NBS **46** (1951).
13. W.G. Van Dorn, J. Mar. Res. **12**, 249 (1953).

14. J.W. Miles, J. Fluid Mech. **3**, 185 (1957).

15. R. Betchov and W.O. Criminale, Jr., *Stability of Parallel Flows*, Academic Press, New York, 1967, p. 27ff.

16. J.W. Miles, J. Fluid Mech. **6**, 568 (1959).

17. J.W. Miles, J. Fluid Mech. **13**, 433 (1962).

18. G.D. Crapper, J. Fluid Mech. **2**, 532 (1957).

19. M.S. Longuet-Higgins and R.W. Stewart, J. Fluid Mech. **8**, 565 (1960).

20. M.S. Longuet-Higgins and R.W. Stewart, J. Fluid Mech. **10**, 529 (1961).